



# A sensorless method for predicting force-induced deformation and surface waviness in robotic milling

Kenan Deng<sup>1</sup> · Dong Gao<sup>1</sup> · Chang Zhao<sup>2</sup> · Yong Lu<sup>1</sup>

Received: 15 December 2022 / Accepted: 4 May 2023 / Published online: 20 May 2023  
© The Author(s), under exclusive licence to Springer-Verlag London Ltd., part of Springer Nature 2023

## Abstract

Process monitoring is essential to enable process parameter optimization, deformation prediction, and fault diagnosis in robotic milling. However, expensive costs and installation requirements limit the use of industrial sensors in machining process. This paper proposed a sensorless method to predict force-induced deformation and surface waviness. First, the tracking errors of tooltip was calculated based on the robot joint tracking errors and the robot kinematic model. Subsequently, the idle running and cutting process signals monitored by the robot controller were used to calculate the cutting force acting on tooltip based on Kalman filter and robot static model. On this base, the force-induced deformation, considering the posture error of the robot flange coordinate system, was calculated using the estimated milling force and the flexible model. Finally, the effectiveness of the proposed method was verified by a series of cutting experiments.

**Keywords** Robotic milling · Sensorless monitoring · Force-induced deformation · Low stiffness · Force estimation · Surface waviness

## Nomenclature

$T_{fl}^{base}$	The transformation from RBCS to RFCS
$\theta_i$	Joint angle around $z$ -axis
$a_i$	The angle measured around the $x$ -axis
$d_i$	Slide distance along the $z$ -axis
$a_i$	The distance along the $x$ -axis
$T_{wp}^{base}$	The transformation from RBCS to WCS
$P_{tool}^{fl}$	The coordinate value of TCP in the RFCS
$M(q)$	The inertia matrix of the robot
$G(q)$	The gravity matrix of the robot
$C(q, \dot{q})$	The centrifugal and Coriolis effects
$\tau_m$	The total joint torque during milling process

$\tau_f$	Joint torque caused by friction
$\tau_{ext}$	Joint torque caused by cutting force (cutting torque)
$\bar{\tau}$	The total joint torque of idle running
$x(t)$	State vector
$y(t)$	Output vector, estimated cutting torque
$u(t)$	Input vector, measured cutting torque
$L$	Kalman gain matrix
$P$	Covariance matrix
$Q$	The covariance of process noise
$R$	The covariance of measurement noise
$J$	Jacobi matrix of the robot
$F_{fl}$	The external force acting in RFCS
$F_{tool}$	The cutting force acting on tooltip
$R_{tool}^{fl}$	The transformation from RFCS to TCS
$PI_i$	The observability index of the $i$ th joint
$\tau_{cut, i}$	The cutting torque of the $i$ th joint
$\tau_{move, i}$	The idle-running torque of the $i$ th joint
$\tau_{ext, m}$	The $n \times 1$ ( $n \geq 3$ ) joint cutting torque matrix
$J_m^T$	The $n \times 6$ generalized Jacobi matrix
$\delta_{fcp}$	The force-induced deformation in the RFCS
$C_\theta$	The robot joint flexibility matrix
$K_\theta$	The robot joint stiffness matrix
$\delta_{tool}$	The deformation of tooltip

✉ Chang Zhao  
zhaochang@connect.hku.hk

✉ Yong Lu  
luyong@hit.edu.cn

Kenan Deng  
1110810922@hit.edu.cn

Dong Gao  
gaodong@hit.edu.cn

<sup>1</sup> School of Mechatronic Engineering, Harbin Institute of Technology, Harbin 150001, China

<sup>2</sup> Department of Mechanical Engineering, The University of Hong Kong, Pokfulam, Hong Kong

## 1 Introduction

Industrial robots have been widely used in applications such as assembly and welding. Also, they are used in machining large parts owing to low cost, high scalability, and large working envelopes [1, 2]. Compared to CNC machine, the low stiffness of industrial robots limits machining quality and efficiency in robotic milling [3, 4]. Excessive milling force are induce high levels of form dimensional errors and surface roughness [5]. Hence, measuring or estimating external forces is an essential task. Process monitoring with extra industrial sensors is an effective method to estimate surface quality [6, 7] and deformation [8]. However, the cost and reliability of installing force/vibration sensors make process monitoring challenging in robotic milling.

Estimating cutting force is an essential part of predicting deformation and is divided into sensor measurement or sensorless estimation methods. In the sensor measurement method, the cutting force can be measured directly by force sensors, such as the table force dynamometer [3], wireless sensors mounted on the tool [4], spindle holder [8], smart tool holder [9], multi-axis force/torque sensing systems attached to the robot flange [10], and torque sensors mounted on the joint side [11]. Sensorless force estimation is achieved using the robot controller's process signals. The researchers extract the external force from the joint signals by separating the joint friction and inertial load when the robot joint motor torque, joint position, velocity, and acceleration are known [12, 13]. Liu and Wang [14] used the joint torque and position provided by the KUKA controller as input values to predict the joint friction force using a neural network and estimate accurate contact force based on a disturbance Kalman filter observer. Huang et al. [15] designed a force estimation observer by fusing a semi-parametric dynamics model with a disturbance Kalman filter by assuming external loads as perturbations. However, these methods are typically used for collaborative robots and are rarely used for heavy-payload industrial robots. In addition, the model-based approach requires obtaining an accurate inertia matrix and friction model. Joint friction is susceptible to load, temperature, and wear state, which increases the difficulty of implementation [16, 17]. For batch machining and handling, the torques of idle and loaded operations can be used to estimate the external load. Yang et al. [18] used robot joint current data before and after loading to predict joint torque for identifying joint stiffness in a heavy-payload industrial robot. Stavropoulos et al. [19] used 'no-load' and 'machining' joint current signals to estimate cutting forces in robotic matching with

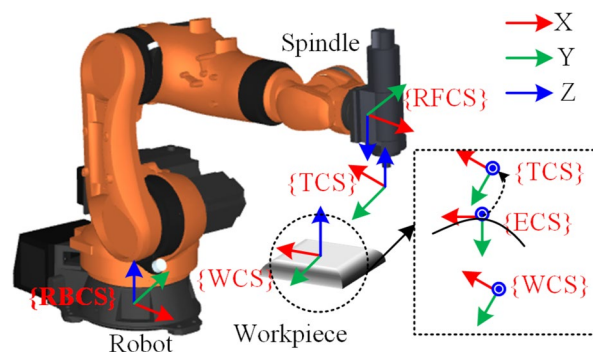


**Fig. 1** KUKA KR160 robot with electric spindle and coordinate system

a 2-degree-of-freedom robot. Nevertheless, it is difficult to effectively measure the torque of each joint caused by the cutting force, resulting in significant errors between the predicted cutting force and the actual value in heavy-payload robotic machining.

The robot stiffness model was used to calculate force-induced deformation [20, 21]. Xiong et al. [3] adjusted feedrate online based on force measurements to reduce machining deformation. Cen et al. [4] proposed a real-time compensation method based on wireless sensors mounted on the tool. Gonzalez et al. [10] used force-torque sensor measurements to predict and compensate for flexible errors with the joint stiffness model. The above studies assumed that the robot flange center position (FCP) errors are the same as the tool center position (TCP) errors. However, the effect of robot posture errors on tooltip should not be ignored when the cutting area is far from the robot flange coordinate system (RFGS).

Prediction of waviness has not been well studied compared to surface roughness [7]. Waviness is mainly caused by low-frequency vibrations in the equipment-tool-workpiece process system [22, 23]. Furtado et al. [24] analyzed the main influencing factors affecting surface waviness through five experiments in robotic milling, using the surface waviness of the workpiece as an indicator of

**Table 1** DH parameters of the KUKA KR160 robot

$i$	$\theta_i(^{\circ})$	$\alpha_i(^{\circ})$	$d_i(\text{mm})$	$a_i(\text{mm})$
1	0	90	500	250
2	90	0	0	610
3	-180	-90	0	70
4	0	90	710	0
5	0	-90	0	0
6	0	0	215	0

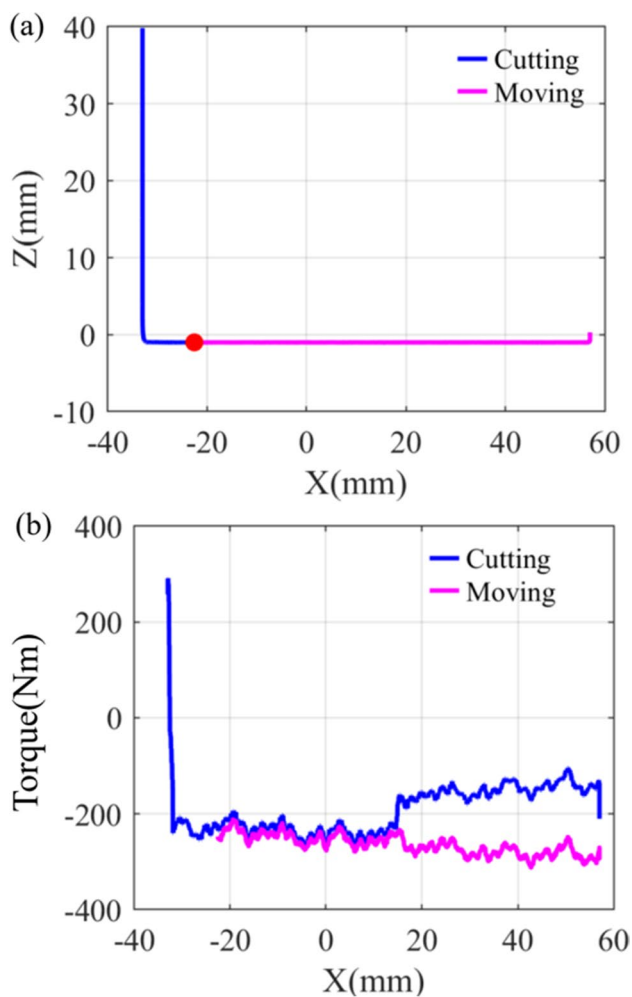


Fig. 2 Signal alignment. (a) Position signals and (b) Torque signals of joint 1

optimizing the robot pose, feed direction, and best process parameters. Surface waviness is usually monitored using external sensors for processes such as grinding [25] and sawing [26]. Liu et al. [27] proposed a multi-sensor fusion method to accurately achieve the online reconstruction of the surface topography of the entire cutting path, including contour and surface roughness. However, the causes and monitoring methods of surface wave formation in robotic milling have not been explored.

In summary, the low stiffness of the industrial robots limit their application in high-precision machining. Offline or online process optimization using measured milling forces is an effective method to improve machining accuracy. However, expensive external force sensors can increase the cost for manufacturing companies. Therefore, there is a need to develop a low-cost approach for estimating milling forces and deformation. The method that estimate external loads based on internal robot data has significant advantages and has been widely used for collaborative or light robots; the method has not been validated for heavy-payload robots due to the significant measurement noise. In addition, waviness is also an important surface accuracy indicator. The formation and prediction of waviness has not been explored in robotic milling. To solve the above problems, a sensorless machining deformation and waviness prediction method is proposed, and the main contributions of this paper are as follows:

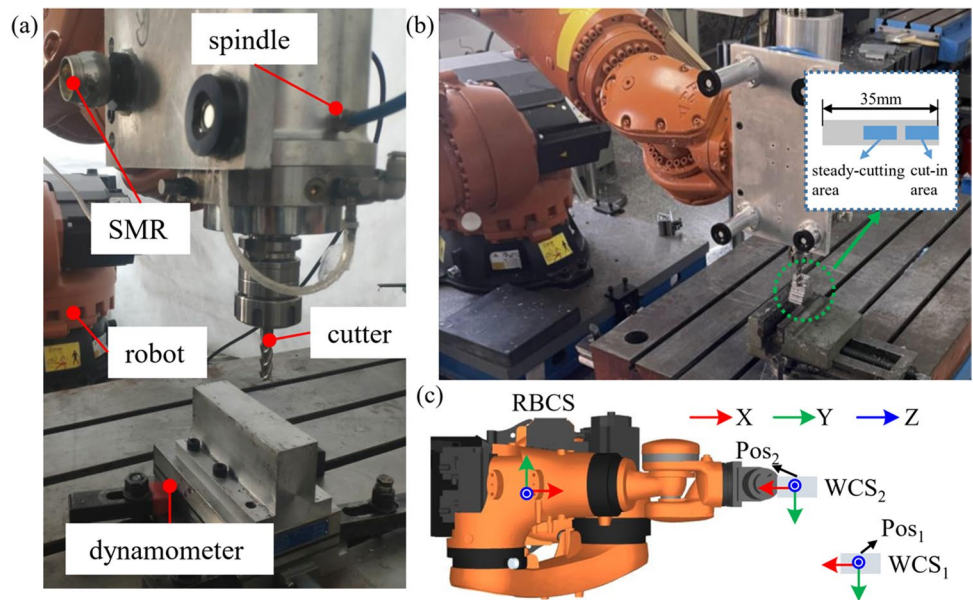
- (1) A sensorless-based milling force acting on tooltip estimation method using internal data of the robot controller is proposed for a heavy-payload industrial robot. The selected joint cutting torque set and robot statics model were used to estimate milling force considering the tooltip-force-induced bending moment of RFCS.
- (2) The tooltip deformation is predicted using the estimated milling force and stiffness model considering the force-induced posture error in the robot flange coordinate system (RFCS) during milling process.
- (3) The formation of waviness is related to the robot tooltip tracking error, which is mainly influenced by the posture error and position error in robotic milling. The robot joint tracking errors and the kinematic model were used to calculate the tooltip tracking error.

The remainder of this paper is organized as follows: Sect. 2 introduces the model of tooltip tracking errors. A method for estimating cutting forces and predicting tooltip’s deformation using process monitoring values recorded by the controller is presented in Sect. 3. Section 4 describes the milling experiments and

Table 2 Joint stiffness of KUKA KR160 Nano robot

Joints	$k_1$	$k_2$	$k_3$	$k_4$	$k_5$	$k_6$
Stiffness (N·m/rad)	1.05e6	1.28e6	1.57e6	0.38e6	0.35e6	0.19e6

**Fig. 3** Experiment setup. **a** Robotic slot milling in pose No. 1. **b** Robotic side milling experiment in pose No. 2. **c** The test pose and its WCS



corresponding results of the KUKA KR-160 robot based on the proposed method. Finally, Sect. 5 summarizes the main results and contributions of this work.

### 2 Robot kinematic and tracking error modeling

As illustrated in Fig. 1, a heavy-payload industrial robot (KUKA KR160 Nano) with an electric spindle mounted on the robot flange was used for modeling and analysis. And the robot base coordinate system (RBCS), the workpiece coordinate system (WCS), the robot flange coordinate system (RFCS), the tool coordinate system (TCS), and the engagement coordinate system (ECS) are defined.

First, the forward kinematic model of the robot is established according to the D-H method [28]; it can be expressed as

$$T_{fl}^{base} = T_6^0 = A_1 A_2 \dots A_6 = \begin{bmatrix} R_{fl}^{base} & P_{fl}^{base} \\ O & 1 \end{bmatrix}, \tag{1}$$

where  $T_{fl}^{base}$  is the transformation from RBCS to RFCS.  $R_{fl}^{base}$  and  $P_{fl}^{base}$  are the rotation matrix and the translation matrix.  $A_i, i = 1, 2 \dots 6$  can be calculated as follows:

$$A_i = \begin{bmatrix} \cos \theta_i & -\sin \theta_i \cos \alpha_i & \cos \theta_i \cos \alpha_i & a_i \cos \theta_i \\ \sin \theta_i & \cos \theta_i \cos \alpha_i & -\cos \theta_i \sin \alpha_i & a_i \sin \theta_i \\ 0 & \sin \alpha_i & \cos \alpha_i & d_i \\ 0 & 0 & 0 & 1 \end{bmatrix}. \tag{2}$$

where  $\theta_i, \alpha_i, d_i,$  and  $\alpha_i$  are the DH parameters of the KUKA KR160 robot and are shown in Table 1.

The encoder sensors installed in the robot are used to record tracking errors between the command and actual positions of the robot axes. KUKA controller provides the KUKA.RobotSensorInterface (RSI) software that enables periodic signal sampling and robot control [29]. This study uses python to develop an interface program to obtain the actual joint position  $\theta_{meas}$  and the commanded joint angle  $\theta_{set}$  with a sampling period of 12 ms. As seen in Fig. 1, the actual Cartesian position and the commanded Cartesian position are calculated according to the robot forward kinematic model and tooltip position in WCS, and the following equation calculates the tracking errors of the FCP:

$$\delta_{tcp} = \left(T_{wp}^{base}\right)^{-T} T_{fl,meas}^{base} \begin{bmatrix} O_{3 \times 1} \\ 1 \end{bmatrix} - \left(T_{wp}^{base}\right)^{-T} T_{fl,set}^{base} \begin{bmatrix} O_{3 \times 1} \\ 1 \end{bmatrix}, \tag{3}$$

where  $T_{wp}^{base}$  is the transformation from RBCS to WCS according to the program value.  $T_{fl,meas}^{base}$  and  $T_{fl,set}^{base}$  are the

**Table 3** Parameters of the cutting tool

Tool no.	Diameter of tool (mm)	Number of teeth	Axial rake angle (°)	Radial rake angle (°)	Helix angles (°)	Overhang (mm)
1	10	3	1	15	30	75
2	16	3	1	15	30	75

**Table 4** Chemical composition of the aluminum alloy 6061-T6

Cu	Si	Fe	Mn	Mg	Zn	Ti	Cr
0.15–0.4%	0.4–0.8%	≤0.7%	≤0.15%	0.80–1.20%	≤0.25%	≤0.15%	0.04–0.35%

transformations from RBCS to RFCS calculated from the actual and commanded joint positions using Eq. (1). The tracking errors of the TCP are influenced by the position errors and posture errors of the RFCS, which are calculated by the following equation:

$$\delta_{\text{tool}} = \left(T_{\text{wp}}^{\text{base}}\right)^{-T} T_{\text{fl, meas}}^{\text{base}} P_{\text{tool}}^{\text{fl}} - \left(T_{\text{wp}}^{\text{base}}\right)^{-T} T_{\text{fl, set}}^{\text{base}} P_{\text{tool}}^{\text{fl}}, \quad (4)$$

where  $P_{\text{tool}}^{\text{fl}}$  is the coordinate value of TCP in the RFCS. It should be noted that tooltip is set as TCP in robotic milling.

### 3 Prediction of force-induced deformation

This paper proposed a sensorless method to estimate cutting forces and tooltip deformation. Considering idle running test is usually performed before actual machining, this paper extracts the cutting force from the process torque and historical torque signals using the Kalman filter method and observability index. Finally, the flexibility model and the estimation values of cutting force were used to predict tooltip deformation.

#### 3.1 Joint torque estimation by Kalman filter

The joint torque can be calculated by the rigid body dynamics model of 6-DOF robot that appears in Eq. (5) [28]:

$$M(q)\ddot{q} + C(q, \dot{q})\dot{q} + G(q) + \tau_f + \tau_{\text{ext}} = \tau_m, \quad (5)$$

where  $M(q)$  and  $G(q)$  are the inertia matrix and gravity matrix and the centrifugal and Coriolis effects are described by  $C(q, \dot{q})$ .  $\tau_m$ ,  $\tau_f$ , and  $\tau_{\text{ext}}$  denote the total joint torque, joint torque caused by friction, and joint torque caused by cutting force (cutting torque). The idle running test effectively verifies the NC program before machining and records historical torque as reference data. On this base, the cutting torque  $\tau_{\text{ext}}$  can be obtained as follows:

$$\tau_{\text{ext}} = \tau_m - \bar{\tau}, \quad (6)$$

where  $\bar{\tau} = M(q)\ddot{q} + C(q, \dot{q})\dot{q} + G(q) + \tau_f$  is the total joint torque of idle running.

This section used the RSI software to acquire joint torque, and the sampling period was 12 ms. The heavy-payload robot does not have joint torque sensors mounted on the joint side, and its torque signal should be estimated using the motor current signal. It is important to emphasize that the idle-running and the milling process signals were not collected synchronously, leading to significant estimation errors. To solve the problem of signal asynchrony, the reference position was set to use the position information to align the idle-running signal with the cutting process signal, as shown in Fig. 2.

The cutting torque is calculated by Eq. (5) using the mean value of the torques of at the specified distance interval (recommended to be greater than 0.5 mm) or the specified time interval. Then a Kalman filter is designed to estimate the actual cutting torque due to the measurement noise. The system can be approximated as a linear time-varying system; therefore, the state space of the discrete system can be written as [30]

$$\begin{cases} \dot{x}(t) = Ax(t) + Bu(t) + w(t) \\ y(t) = Hx(t) + v(t) \end{cases}, \quad (7)$$

where  $x(t)$ ,  $y(t)$ , and  $u(t)$  are the state vector, output vector (estimated cutting torque), and input vector (measured cutting torque), respectively.  $u(t)$  can be obtained using Eq. (6).  $A$ ,  $B$ , and  $H$  are called the state matrices and are given as

$$A = I, H = I, B = I. \quad (8)$$

Kalman gain matrix  $L$  and covariance matrix  $P$  of the sensor system are identified by minimizing the state estimation error covariance and using the Riccati equation:

$$L = PH^T R^{-1}, \quad (9)$$

$$AP + PA^T - PH^T HP^T R^{-T} + BQB^T, \quad (10)$$

where  $Q$  and  $R$  are the covariance of process noise and measurement noise.

**Table 5** Experimental details and cutting parameters

Test no.	Tool no.	Pose no.	Spindle speed (rpm)	Feed per tooth (mm)	Axial depth of cut (mm)	Radial width of cut (mm)
1, 2, 3	1	1	4500	0.05	1, 2, 3	10
4, 5, 6	2	2	1800, 3600, 5400	0.05	5	2

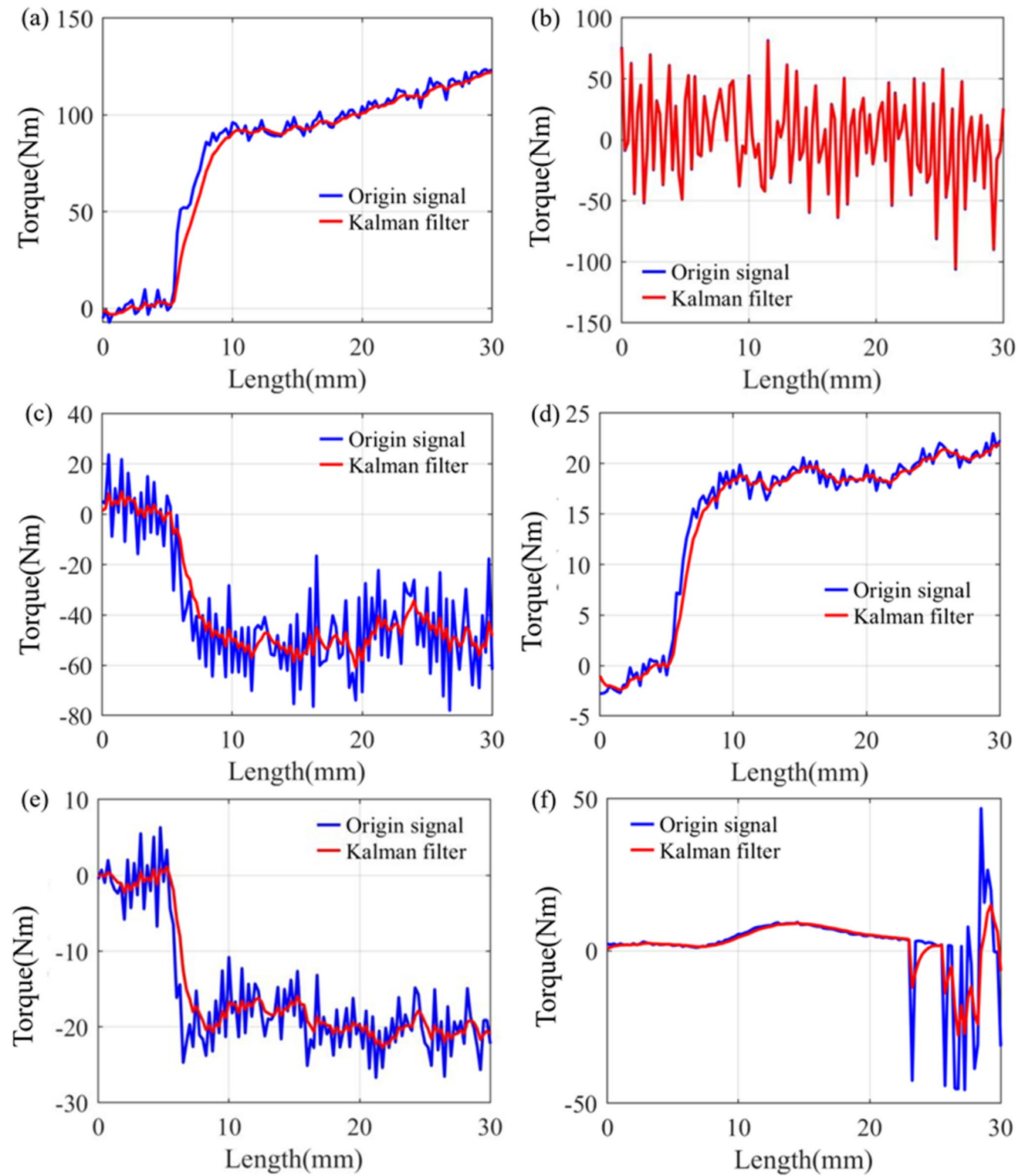


**Fig. 4** Raw and filtered values of cutting torque for **a** joint 1, **b** joint 2, **c** joint 3, **d** joint 4, **e** joint 5, and **f** joint 6 in test No. 1

**Table 6** The covariance matrix of measurement noise and system noise

Axis	$Q$	$R$
1	0.193	7.645
2	0.392	15.693
3	0.295	8.766
4	0.0135	1.0626
5	0.032	2.123
6	0.0232	2.076

### 3.2 Cutting force estimation based on static model

The joint torque caused by external force can be calculated from the Jacobi matrix and external force using based on the static model of the robots [28]:

$$\tau_{ext} = J^T F_{fl}, \tag{11}$$

where  $J$  is the Jacobi matrix of the robot and  $F_{fl}$  is the external force acting in RFCS, which is described as  $F_{fl} = [F_{fl,x}, F_{fl,y}, F_{fl,z}, M_{fl,x}, M_{fl,y}, M_{fl,z}]^T$ .  $F_{fl}$  can be calculated by the coordinate conversion below based on the cutting force of tooltip  $F_{tool}$ .

$$F_{fl} = R_{tool}^{fl} F_{tool}, \tag{12}$$

where  $F_{tool} = [F_{tool,x}, F_{tool,y}, F_{tool,z}]^T$  and  $R_{tool}^{fl}$  is the transformation from RFCS to TCS and is calculated as

$$R_{tool}^{fl} = \begin{bmatrix} 0 & 0 & -1 & 0 & -P_{tool,z} & 0 \\ 0 & -1 & 0 & P_{tool,z} & 0 & -P_{tool,x} \\ -1 & 0 & 0 & 0 & P_{tool,x} & 0 \end{bmatrix}^T, \tag{13}$$

where  $P_{tool,x}$  and  $P_{tool,z}$  are the coordinate values of tooltip under the RFCS.  $P_{tool,y}$  can be ignored in the calculation.

For heavy-payload robots, it is difficult to effectively estimate the cutting force when the cutting torque is smaller than the torque fluctuation (torque measurement noise) caused by joint friction and inertial load. To reduce the estimation error, it is necessary to reasonably select the joint torques for calculation according to the cutting torque measurement value and the measurement noise. Hence, the observability index is expressed as

$$PI_i = \frac{\text{abs}(\text{mean}(\tau_{cut,i}))}{\max(\tau_{move,i}) - \min(\tau_{move,i})}, \tag{14}$$

where  $\tau_{cut,i}$  and  $\tau_{move,i}$  are the cutting and idle-running torques of the  $i$ th joint.  $PI_i$  describes the observability of the  $i$ th joint cutting torque measurement, and the threshold value is set to 2. Robot joints with observability indexes greater than the threshold are used for subsequent force estimation, and the cutting force in the TCS is calculated by substituting Eqs. (12) and (13) into Eq. (11), which is

$$F_{tool} = (J_m^T R_{tool}^{fl})^{-1} \tau_{ext,m}, \tag{15}$$

where  $\tau_{ext,m}$  and  $J_m^T$  are the  $n \times 1$  ( $n \geq 3$ ) joint torque matrix and the  $n \times 6$  generalized Jacobi matrix corresponding to the selected joints. When less than three-joint torque data are available for measurement, it is difficult to calculate the three-direction milling force by Eq. (15).

### 3.3 Deformation prediction considering posture errors

A robot flexibility model based on the assumption of a single degree of freedom linear spring was used to calculate

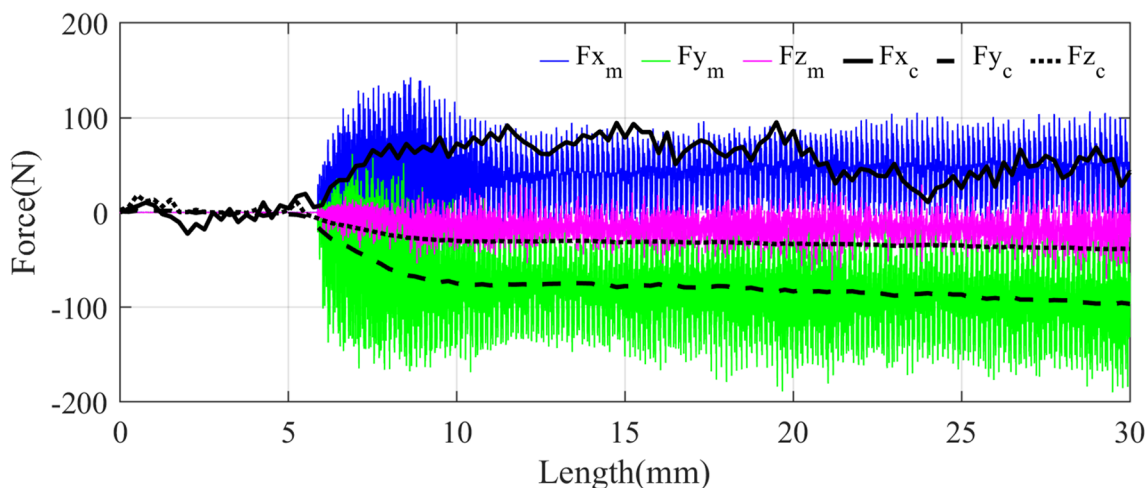


**Fig. 5** Estimated and measured milling force values in test No. 1

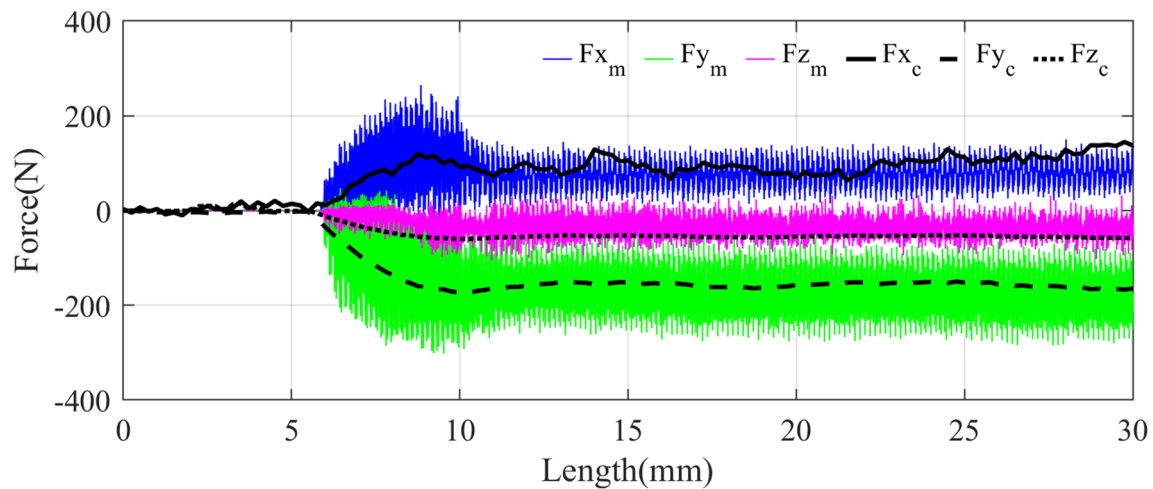


**Fig. 6** Estimated and measured milling force values in test No. 2

force-induced deformation in the RFCS using Eq. (16) when the cutting torque of each joint is effectively observed.

$$\delta_{fcp} = JC_{\theta}\tau_{ext}, \quad (16)$$

where  $C_{\theta}$  is the robot flexibility matrix that can be described by  $C_{\theta} = K_{\theta}^{-1}$ , where  $K_{\theta}$  is the robot joint stiffness matrix  $K_{\theta} = \text{diag}([k_1, k_2, k_3, k_4, k_5, k_6])$ . In general, only the cutting torques of 3 to 4 joints can be used for estimation. By inserting Eq. (15) into Eq. (16), the deformation can be calculated as follow:

$$\delta_{fcp} = JCJ^T R_{tool}^{\theta} F_{tool}. \quad (17)$$

The posture error is usually neglected in the calculation of force-induced deformation. Hence, the deformation of tooltip is assumed to be the same as the

deformation of FCP [3, 4, 10, 18, 20]. However, the influence of the posture error of FCP on the position error of tooltip cannot be neglected, considering the distance between tooltip and the FCP. As a result, the deformation of tooltip is obtained by the following equation:

$$\delta_{tool} = \begin{bmatrix} 0 & 0 & -1 & 0 & -P_{tool,z} & 0 \\ 0 & -1 & 0 & P_{tool,z} & 0 & -P_{tool,x} \\ -1 & 0 & 0 & 0 & P_{tool,x} & 0 \end{bmatrix} \delta_{fcp}. \quad (18)$$

Although the joints of the robot have obvious non-linear characteristics, many researchers assume that the stiffness of the joints is a linear constant-value spring. And the machining deformation predicted by this linear model can meet the accuracy requirements in robotic milling [1, 3, 4, 10, 18, 20]. According to

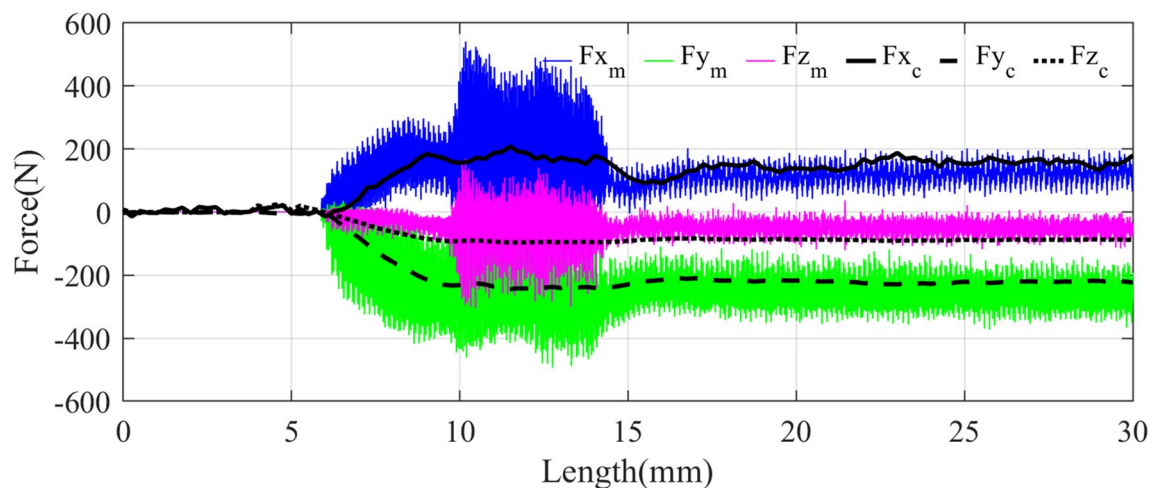


**Fig. 7** Estimated and measured milling force values in test No. 3



**Table 7** Mean values of measured and estimated milling forces in TCS

Test no.	Milling force in the X direction $F_x$ (N)			Milling force in the Y direction $F_y$ (N)			Milling force in the Z direction $F_z$ (N)		
	Measurement	Estimation	Errors (%)	Measurement	Estimation	Errors (%)	Measurement	Estimation	Errors (%)
1	45.96	56.21	22.3	-96.10	-84.73	11.83	-18.21	-33.89	86.11
2	78.125	102.71	31.47	-176.50	-157.15	10.96	-34.71	-54.66	57.5
3	150.75	127.13	15.67	-266.83	-223.07	16.40	-51.65	-89.23	72.76

the method proposed in references [20, 21], the identification results of the robot joint stiffness are shown in Table 2.

## 4 Experiment and discussion

To verify the effectiveness of the proposed method in this paper, a series of cutting experiments were conducted using a KUKA KR 160 robot whose rated payload and pose repeatability are 160 kg and  $\pm 0.06$  mm. As shown in Fig. 3 (a) and (b), an electric spindle, whose maximum speed and rated torque are 16,000 rpm and 6 Nm, was mounted on the robot flange. Robotic milling experiments were conducted at different pose. The poses and its WCS of two experiments are indicated in Fig. 3(c). The tool parameters and chemical composition of the workpiece (aluminum alloy 6061-T6) are listed in Tables 3 and 4, respectively. Table 5 lists the experimental details and cutting parameters. The maximum radial run-out of the tooltip of the tool no. 1 was measured by a dial indicator and was  $7.35 \mu\text{m}$ . The axial and radial runouts of the tooltip usually affect the instantaneous milling force of each tooth [31, 32]. The low measurement bandwidth of the robot joint torque makes it difficult to predict the instantaneous milling force acting on the tooltip, so the effect of the tool runout value on the predicted forces can be ignored.

### 4.1 Robotic slot milling experiment

Test No. 1 to No. 3 were used to verify the force estimation method proposed in Sects. 3.1 and 3.2. As shown in Fig. 3(a), the tool fed along the  $x$ -direction in WCS. Kistler 9257B dynamometer was used to measure milling force for comparison with estimation forces. The force components were defined in the TCS as  $y$  — feed normal force  $F_y$ ,  $x$  — feed force  $F_x$ , and  $z$  — thrust force  $F_z$ . The measured forces were converted from the WCS into the TCS based on the kinematic model and calibration conversion between MCS and RBCS (Fig. 1).

The measured and filtered cutting torques for six joints in test No. 1 were compared in Fig. 4. The

parameters of Kalman filters were designed using measured joint torques. The measurement noise covariance  $\mathbf{R}$  of Eq. (10) are determined according to the root mean square of the idle running data, and the process noise covariance  $\mathbf{Q}$  of Eq. (10) are adjusted accordingly to improve the identification accuracy. The covariance matrix of measurement noise and system noise of each axis is taken as shown in Table 6. As can be seen, the observed cutting torques for joint 1 and joint 4 were more significant, and measurement noise had minimal effect. The torque signal of the cutting process contains three parts: air cutting, cut-in process, and steady cutting. It can also be observed obviously that the joint torque gradually increases as the tool cuts into the material. The filtered torques for joint 3 and joint 5 with greater measurement noise could also be used for estimating cutting force compared to the filtered torque of joint 1. Cutting torques could not be observed from the signals of joint 2 and joint 6.

The estimated and measured values of the three-direction milling forces in TCS were compared in Figs. 5, 6, and 7 using the proposed method in Sect. 3.2. The estimated milling forces using the robot controller's torque signals could capture the cut-in workpiece, steady cutting, and cut-leave workpiece processes. However, the predicted values cannot accurately reflect the cyclic fluctuation of milling forces. The estimated force  $F_{x_c}$

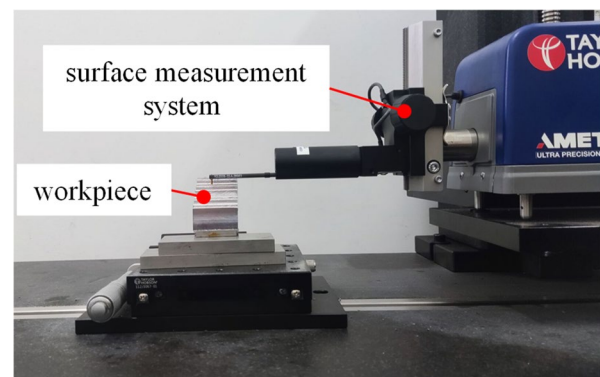


**Fig. 8** Using Taylor Form Talysurf inductive to measure the workpiece surface

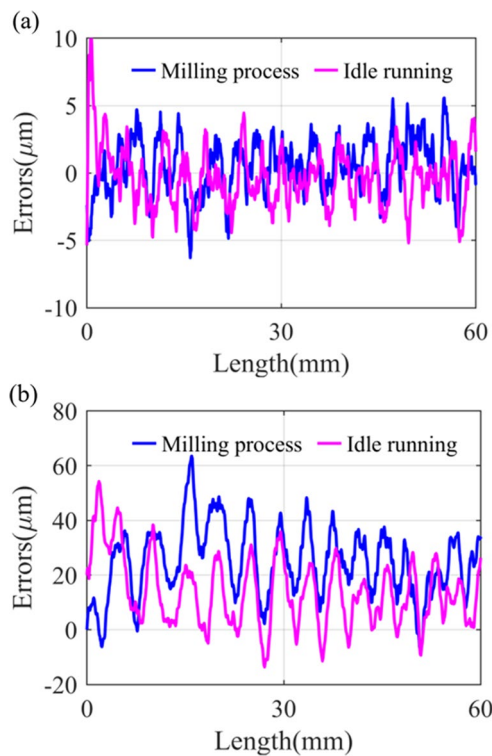


**Fig. 9** Tracking error during the cutting process and idle running in test No. 5. **a** Tracking error of FCP. **b** Tracking error of tooltip

was more susceptible to joint torque measurement noise and had larger fluctuations than other  $F_{y_c}$  and  $F_{z_c}$ . In addition, there were computation residuals during the air cutting process owing to measurement noise, when the actual milling force should be zero.

Table 7 compares the mean measured and the mean estimated forces of three directions in the selected cutting area (15–25 mm) in test No. 1, No. 2, and No. 3. As can be seen, both the average of the measured milling forces and the estimated milling forces were linearly

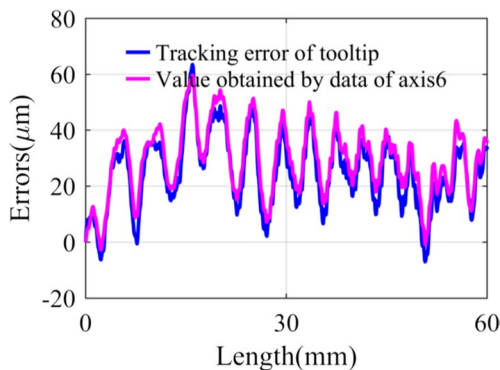


**Fig. 10** Comparison of tooltip tracking errors and tooltip errors calculated by joint 6 tracking errors in test No. 5

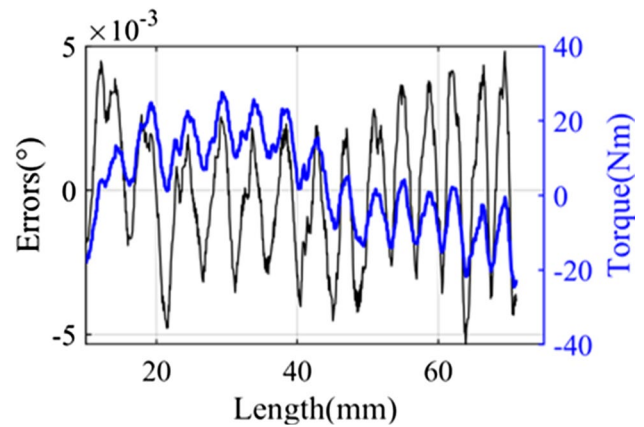


**Fig. 11** Comparison of joint 6 tracking errors and joint 6 torque in test No. 5

related to the axial depth of cut. In general, the estimated milling forces  $F_{x_c}$  and  $F_{y_c}$  were lower than the measured values. In contrast, the estimated values in the  $F_{z_c}$  were higher. As shown in Table 7, the estimated forces deviate from the average measured forces primarily due to the following reasons: (1) the joint torque measurement bandwidth and measurement error provided by the robot controller are significant, to accurately measure high-frequency milling force signals. (2) The transmission of cutting force from tooltip to each joint is affected by geometric errors, deformation, backlash, friction, and other factors. (3) The average force is used as a reference value and is not reflective of the true load on each joint of the robot under high-frequency milling forces [3–7, 15, 17]. Therefore, although there is a significant difference between the estimated milling force acting on the tooltip using joint torque and the measured milling force, it is considered to be more reflective of the actual loads imposed on the robot joints by the milling force [18].

## 4.2 Robotic sliding milling experiment

In accordance with the cutting parameters recorded in Table 5, test No. 4, No. 5, and No. 6 were used to verify the deformation prediction and surface wave formation. Figure 3(b) shows that a 16-mm-diameter carbide end mill with 3-tooth was used to conduct a robotic side milling experiment at different spindle speeds and the tool fed along  $x$ -direction of TCS. The cutting length of the aluminum alloy workpiece was 35 mm. Taylor Form Talysurf inductive (Fig. 8) was used to measure the surface contours of the cut-in area (0–10 mm from the entry point) and steady-cutting area (12.5–22.5 mm from the entry point). The cut-in area and steady-cutting area can be shown in Fig. 3(b).

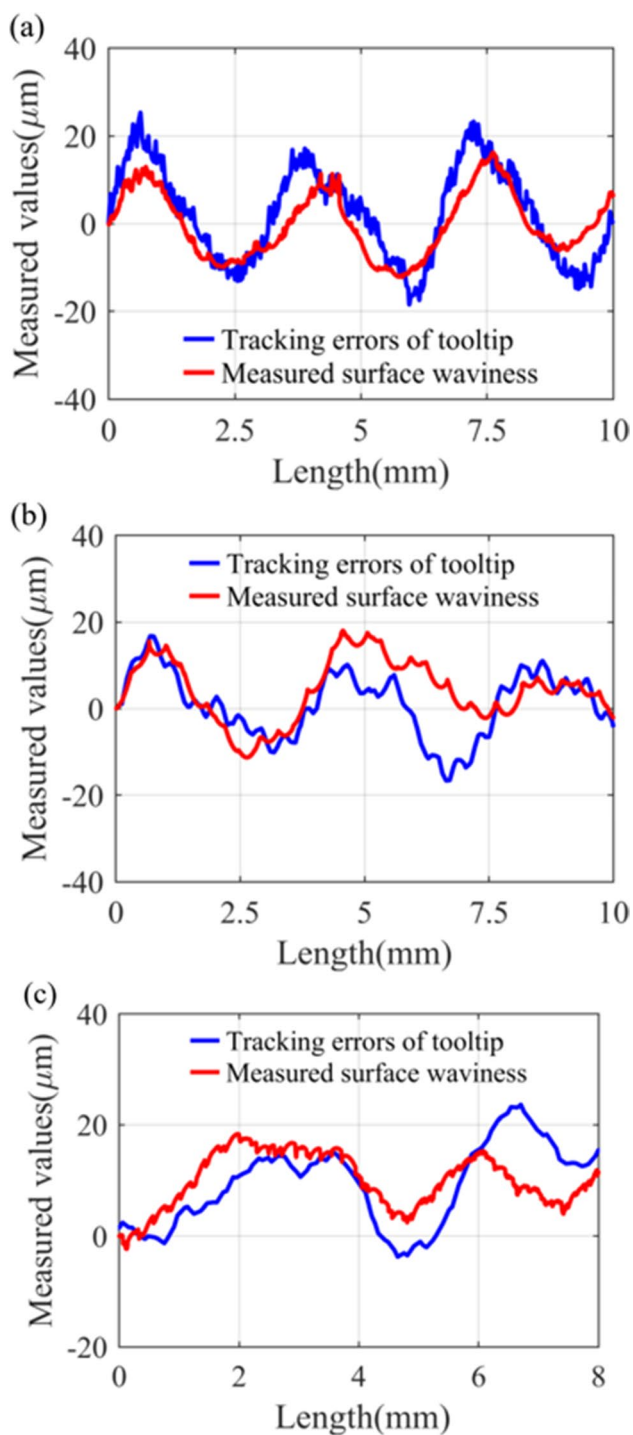


**Fig. 12** Comparison of surface waviness and tooltip tracking errors in **a** test No. 4, **b** test No. 5, and **c** test No. 6

Figure 9(a) compares the tracking errors of FCP in the y-direction of TCS at idle running and cutting process in test No. 5 using the Eq. (3). And the tracking errors of tooltip, calculated from Eq. (4), are analyzed in

Fig. 9(b). It can be seen that the tracking errors of tooltip were much larger than the values of FCP. The tracking error amplitudes of tooltip were approximately 40 μm, while the tracking error amplitudes of FCP were about 10 μm. Consequently, the robot posture errors of FCS significantly impact the tracking errors of tooltip. Also, the tracking errors during the cutting process and idle running were similar because the milling force excitation frequency was higher than the natural frequency of the robot structure.

Tracking error calculated by all joints' tracking errors and joint 6 tracking errors are analyzed in Fig. 10, and it can be seen that joint 6 tracking errors is an essential factor in the tracking errors of tooltip, compared to the error of FCP (Fig. 9). Figure 11 shows that the torque curve of joint 6 is similar to the tracking error curve of joint 6. That means that the torque fluctuation of joint 6 is mainly caused by friction when machining small-sized workpieces at low feedrate. The acceleration of joint 6 remains stable, and the variation of inertial and gravitational loads can be negligible. It should be noted that the variation of the velocity direction of joint 6 at 50.9 mm leads to the variation in the joint torque value.

The tracking errors of tooltip and surface profile measurements of steady cutting areas are compared in Fig. 12 (test No. 4 to No. 6). The measured waviness curves of the workpiece surface were similar to the tracking error curves of tooltip, so the formation of waves on the workpiece surface is related to the operating state of the robot. Combined with the previous analysis, the tracking errors of tooltip, which are obtained in the idle running and cutting process, can be used to predict the surface waviness in robotic side milling. This means we can obtain the machining parameters for optimal surface waviness by monitoring tooltip tracking errors through idle running tests before formal machining without cutting experiments.

The milling force of the side milling was calculated using the filtered cutting torque based on the proposed method in Sects. 3.1 and 3.2. Figure 14(d) shows the estimated three-direction milling force using the selected robot joints' cutting torque. Compared with test 1 (Fig. 4), the torque measurement noise of joint 3 was increased, while the noise of joint 6 was decreased. Therefore, the cutting torques of joint 1, joint 5, and joint 6 were used for estimating milling force acting on tooltip.

Figures 14(a), 15(a), and 16(a) show the predicted tooltip force-induced deformation curves, calculated from Eq. (18), using estimated milling forces. It can be seen that tooltip deformation gradually increases

**Fig. 13** Joint cutting torque measurement and estimated milling force in test No. 5. Cutting torque values of **a** robot joint 1, **b** joint 5, and **c** joint 6 and **d** predicted milling force value

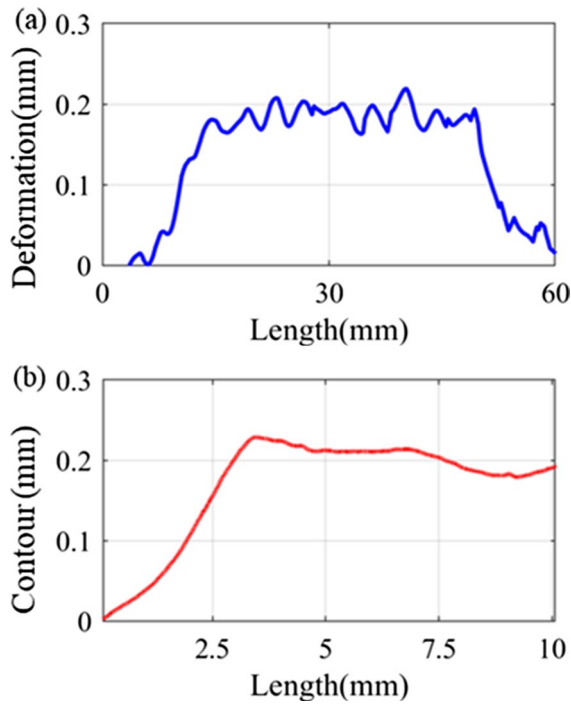
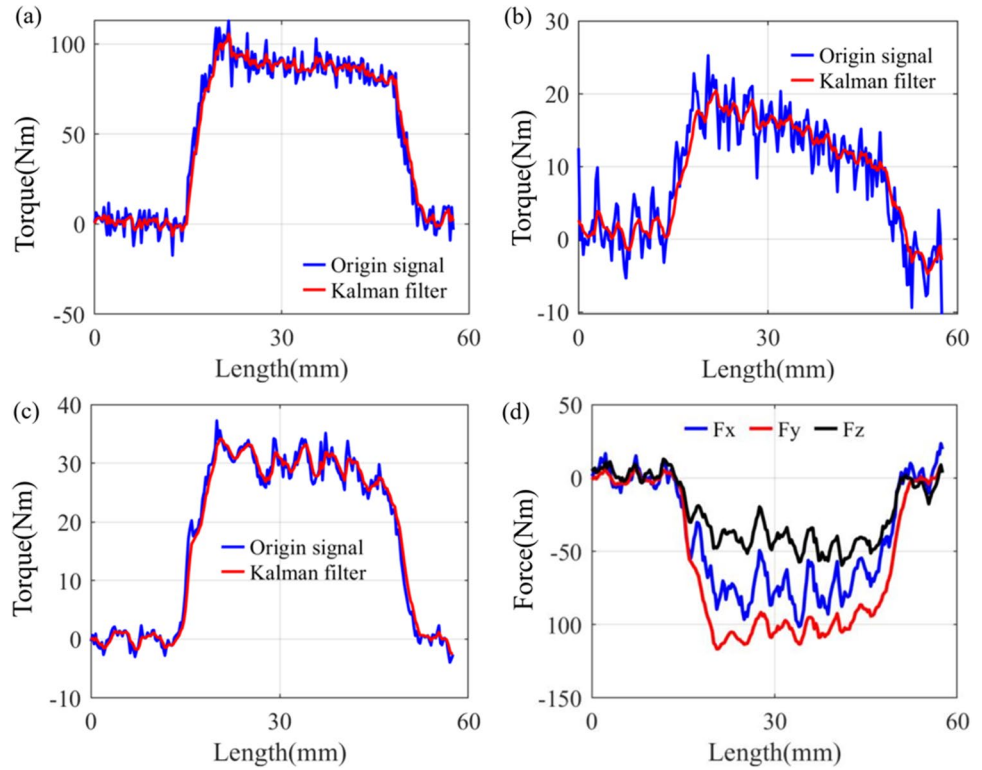


**Fig. 14** Comparison of predicted tooltip deformation and measured workpiece surface contour in test No. 4. **a** Predicted tooltip deformation and **b** measured workpiece surface contour in cut-in area of the workpiece

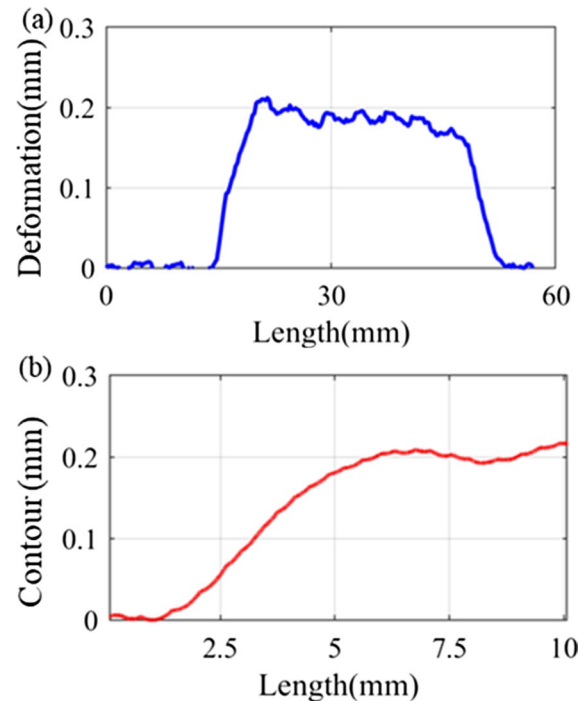


**Fig. 15** Comparison of predicted tooltip deformation and measured workpiece surface contour in test No. 5. **a** Predicted tooltip deformation and **b** measured workpiece surface contour in cut-in area of the workpiece

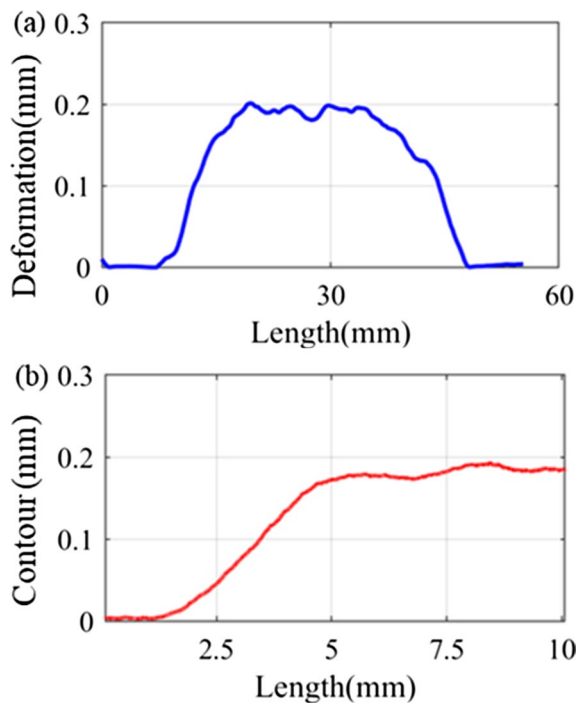


**Fig. 16** Comparison of predicted tooltip deformation and measured workpiece surface contour in test No. 6. **a** Predicted tooltip deformation and **b** measured workpiece surface contour in cut-in area of the workpiece

during the tool cutting into the workpiece and gradually decreases when the tool cut-leave the workpiece. The predicted value fluctuates mainly due to the fluctuation of the estimated forces caused by the measurement noise. However, there are fluctuations in the predicted curves during air cutting, mainly related to the estimated force errors (see Fig. 13(d)). Figures 14(b), 15(b), and 16(b) depict the contour of the tool cutting into the workpiece, and it can be seen that the contour changes as the tool cuts into the workpiece, and the workpiece contour error is almost constant when in the steady cutting process. The predicted and measured values in Table 8 are the average values of the deformation in the steady cutting area after the tool is completely cut into the workpiece to reduce the influence of surface waviness, and the prediction error is below 11% (<0.02 mm), which can meet the actual machining requirements.

**Table 8** Measured surface errors and predicted tooltip deformation

Test no.	Tooltip deformation (mm)		
	Measurement	Prediction	Errors
4	0.203	0.182	10.35%
5	0.206	0.192	6.80%
6	0.175	0.194	10.86%

## 5 Conclusions

In this paper, a sensorless method for predicting tooltip deformation and surface waviness is proposed, and the main contributions of this paper can be summarized as follows:

The cutting forces acting on tooltip were estimated using selected joint torques provided by the robot controller based on the Kalman filter method and observability index. Robotic slot milling experiments were used to validate the proposed method, and the estimated cutting forces were close to the average of the reference values measured by a force dynamometer.

The estimated milling force and the flexible model were used to predict the force-induced deformation of tooltip, considering the robot posture error of FCS. Compared with the measured data from the surface profiler, the machining deformation prediction errors at the steady cutting areas were less than 11% (<0.02 mm), which meets the accuracy requirement.

The estimated cutting force and deformation curves distinguish the process of air cutting, the cut-into workpiece, steady cutting, and cut-leave workpiece during milling process.

The cutting experiments proved that the formation of surface waviness in robotic side milling is closely related to the tracking errors of tooltip. The robot posture error caused by the joint 6 friction is an important cause of the tracking errors of tooltip when the robot feed along the *x*-direction of the TCS.

Real-time sensorless deformation compensation method for curved workpiece considering pose-oriented stiffness model will be further investigated.

**Code availability** Not applicable.

**Author contributions** K. N. D., Y. L., and D. G. conceived and designed the study. K. N. D. and S. D. M. performed the experiments. K. N. D. and C. Z. wrote the paper. K. N. D., Y. L., and D. G. reviewed and edited the manuscript. All authors read and approved the manuscript.

**Funding** This work was supported by National Key Research and Development Project of China (2018YFB1306803).

**Data availability** The publication-related datasets are available from the corresponding author on reasonable request.

## Declarations

**Ethics approval** Not applicable.

**Consent to participate** Not applicable.

**Consent for publication** All authors approved the manuscript and gave their consent for submission and publication.

**Competing interests** The authors declare no competing interests.

## References

- Verl A, Valente A, Melkote S et al (2019) Robots in machining. *CIRP Annals* 68(2):799–822. <https://doi.org/10.1016/j.cirp.2019.05.009>
- Deng K, Gao D, Zhao C, Yong L (2023) Prediction of in-process frequency response function and chatter stability considering pose and feedrate in robotic milling. *Robot Comput Integr Manuf* 82:102548. <https://doi.org/10.1016/j.rcim.2023.102548>
- Xiong G, Li ZL, Ding Y, Zhu L (2020) Integration of optimized feedrate into an online adaptive force controller for robot milling. *Int J Adv Manuf Technol* 106(3):1533–1542. <https://doi.org/10.1007/s00170-019-04691-1>
- Cen L, Melkote SN, Castle J, Howard A (2016) A wireless force-sensing and model-based approach for enhancement of machining accuracy in robotic milling. *IEEE ASME Trans Mechatron* 21(5):2227–2235. <https://doi.org/10.1109/TMECH.2016.2567319>
- Wojciechowski S, Matuszak M, Powalka B, Madajewski M, Maruda RW, Królczyk GM (2019) Prediction of cutting forces during micro end milling considering chip thickness accumulation. *Int J Mach Tools Manuf* 147:103466. <https://doi.org/10.1016/j.ijmachtools.2019.103466>
- Wojciechowski S, Maruda RW, Krolczyk GM, Niestony P (2018) Application of signal to noise ratio and grey relational analysis to minimize forces and vibrations during precise ball end milling. *Precis Eng* 51:582–596. <https://doi.org/10.1016/j.precisioneng.2017.10.014>
- Wojciechowski S, Wiackiewicz M, Krolczyk GM (2018) Study on metrological relations between instant tool displacements and surface roughness during precise ball end milling. *Measurement* 129:686–694. <https://doi.org/10.1016/j.measurement.2018.07.058>
- Denkena B, Lepper T (2015) Enabling an industrial robot for metal cutting operations. *Procedia CIRP* 35:79–84. <https://doi.org/10.1016/j.procir.2015.08.100>
- Zhang P, Gao D, Lu Y, Wang F, Liao Z (2022) A novel smart toolholder with embedded force sensors for milling operations. *Mech Syst Signal Process* 175:109130. <https://doi.org/10.1016/j.ymsp.2022.109130>
- Gonzalez MK, Theissen NA, Barrios A, Archenti A (2022) Online compliance error compensation system for industrial manipulators in contact applications. *Robot Comput Integr Manuf* 76:102305. <https://doi.org/10.1016/j.rcim.2021.102305>
- Stürz YR, Affolter LM, Smith RS (2017) Parameter identification of the KUKA LBR iiwa robot including constraints on physical feasibility. *IFAC-PapersOnLine* 50(1):6863–6868
- Wahrburg A, Bös J, Listmann KD, Dai F, Matthias B, Ding H (2017) Motor-current-based estimation of cartesian contact forces and torques for robotic manipulators and its application to force control. *IEEE Trans Autom Sci Eng* 15(2):879–886. <https://doi.org/10.1109/TASE.2017.2691136>
- Zhang S, Wang S, Jing F, Tan M (2019) A sensorless hand guiding scheme based on model identification and control for industrial robot. *IEEE Trans Industr Inform* 15(9):5204–5213. <https://doi.org/10.1109/TII.2019.2900119>
- Liu S, Wang L, Wang XV (2021) Sensorless force estimation for industrial robots using disturbance observer and neural learning of friction approximation. *Robot Comput Integr Manuf* 71:102168. <https://doi.org/10.1016/j.rcim.2021.102168>
- Huang J, Zhang M, Ri S, Xiong C, Li Z, Kang Y (2019) High-order disturbance-observer-based sliding mode control for mobile wheeled inverted pendulum systems. *IEEE Trans Ind Electron* 67(3):2030–2041. <https://doi.org/10.1109/TIE.2019.2903778>
- Bittencourt AC, Axelsson P (2013) Modeling and experiment design for identification of wear in a robot joint under load and temperature uncertainties based on friction data. *IEEE ASME Trans Mechatron* 19(5):1694–1706. <https://doi.org/10.1109/TMECH.2013.2293001>
- Bittencourt AC, Gunnarsson S (2012) Static friction in a robot joint—modeling and identification of load and temperature effects. *J Dyn Syst Meas Control* 134(5). <https://doi.org/10.1115/1.4006589>
- Yang K, Yang W, Cheng G, Lu B (2018) A new methodology for joint stiffness identification of heavy duty industrial robots with the counterbalancing system. *Robot Comput Integr Manuf* 53:58–71. <https://doi.org/10.1016/j.rcim.2018.03.001>
- Stavropoulos P, Bikas H, Souflas T, Ghassempouri M (2021) A method for cutting force estimation through joint current signals in robotic machining. *Procedia Manuf* 55:124–131. <https://doi.org/10.1016/j.promfg.2021.10.018>
- Abele E, Weigold M, Rothenbücher S (2007) Modeling and identification of an industrial robot for machining applications. *CIRP Annals* 56(1):387–390. <https://doi.org/10.1016/j.cirp.2007.05.090>
- Bu Y, Liao W, Tian W, Zhang J, Zhang L (2017) Stiffness analysis and optimization in robotic drilling application. *Precis Eng* 49:388–400. <https://doi.org/10.1016/j.precisioneng.2017.04.001>
- Yue C, Gao H, Liu X, Liang SY (2018) Part functionality alterations induced by changes of surface integrity in metal milling process: a review. *Appl Sci* 8(12):2550. <https://doi.org/10.3390/app8122550>
- Grzesik W (2008) Advanced machining processes of metallic materials: theory, modeling and applications. Elsevier
- Furtado LFF, Villani E, Trabasso LG, Suterio R (2017) A method to improve the use of 6-dof robots as machine tools. *Int J Adv Manuf Technol* 92(5):2487–2502. <https://doi.org/10.1007/s00170-017-0336-8>
- Ahrens M, Fischer R, Dagen M, Denkena B, Ortmaier T (2013) Abrasion monitoring and automatic chatter detection in cylindrical plunge grinding. *Procedia CIRP* 8:374–378. <https://doi.org/10.1016/j.procir.2013.06.119>
- Nasir V, Cool J, Sassani F (2019) Acoustic emission monitoring of sawing process: artificial intelligence approach for optimal sensory feature selection. *Int J Adv Manuf Technol* 102(9):4179–4197. <https://doi.org/10.1007/s00170-019-03526-3>
- Liu C, Gao L, Wang G, Xu W, Jiang X, Yang T (2020) Online reconstruction of surface topography along the entire cutting path in peripheral milling. *Int J Mech Sci* 185:105885. <https://doi.org/10.1016/j.ijmecsci.2020.105885>
- Schreoder K (1999) Handbook of industrial robotics. John Wiley & Sons. <https://doi.org/10.1002/9780470172506>
- Deng K, Gao D, Ma S, Zhao C (2023) Elasto-geometrical error and gravity model calibration of an industrial robot using the same optimized configuration set. *Robot Comput Integr Manuf* 83:102558. <https://doi.org/10.1016/j.rcim.2023.102558>
- Aslan D, Altintas Y (2018) Prediction of cutting forces in five-axis milling using feed drive current measurements. *IEEE ASME Trans Mechatron* 23(2):833–844. <https://doi.org/10.1109/TMECH.2018.2804859>
- Chen Y, Lu J, Deng Q, Ma J, Liao X (2022) Modeling study of milling force considering tool runout at different types of radial cutting depth. *J Manuf Process* 76:486–503. <https://doi.org/10.1016/j.jmapro.2022.02.037>
- Yue C, Gao H, Liu X, Liang SY (2019) A review of chatter vibration research in milling. *Chinese J Aeronaut* 32(2):215–242. <https://doi.org/10.1016/j.cja.2018.11.007>

**Publisher's note** Springer Nature remains neutral with regard to jurisdictional claims in published maps and institutional affiliations.

Springer Nature or its licensor (e.g. a society or other partner) holds exclusive rights to this article under a publishing agreement with the author(s) or other rightsholder(s); author self-archiving of the accepted manuscript version of this article is solely governed by the terms of such publishing agreement and applicable law.